
Article:
Handley, C.M. orcid.org/0000-0001-7291-2197, Gao, E., Heath, J.P. et al. (2 more authors) (2023) Understanding the structure-dielectric property relationships of (Ba0.8Ca0.2)TiO3-Bi(Mg0.5Ti0.5)O3 perovskites. Acta Materialia, 246. 118649. ISSN: 1359-6454

https://doi.org/10.1016/j.actamat.2022.118649

Acta Materialia 246 (2023) 118649

Contents lists available at ScienceDirect

Acta Materialia

journal homepage: www.elsevier.com/locate/actamat

Understanding the structure-dielectric property relationships of $(Ba_{0.8}Ca_{0.2})TiO_3$-$Bi(Mg_{0.5}Ti_{0.5})O_3$ perovskites

Christopher M. Handley [a], Erze Gao [b], James P. Heath [a], Derek C. Sinclair [a], Colin L Freeman [a,*]

[a] Department of Materials Science and Engineering, University of Sheffield, Mappin Street, Sheffield S1 3JD, UK
[b] Department of Chemistry, University College London, Gordon Street, WC1H 0AJ, UK

ARTICLE INFO

Keywords:
Functional ceramics
Ferroelectric relaxor
Solid solutions
Capacitor
Lead-free ceramics

Atomic-level simulations are used to examine the structure, thermodynamics, and dielectric properties of $(Ba_{0.8}Ca_{0.2})TiO_3$-$Bi(Mg_{0.5}Ti_{0.5})O_3$ perovskites. These simulations demonstrate that mixing is non-ideal between the end-members, and only specific configurations can form at higher $Bi(Mg_{0.5}Ti_{0.5})O_3$ content. Significant structural relaxations are identified around the Bi and Mg cations. The effect of these relaxations on polarization is investigated and highlights that they disrupt ferroelectric domains in the material, preventing collective polarization mechanisms that links to the experimentally observed relatively flat permittivity-temperature profiles [1].

1. Introduction

Functional oxide ceramics represent a key class of materials in our modern world, making up, for example, the passive components of many devices such as capacitors, micro-positioners, sensors, etc. There is a continuous drive to improve the dielectric properties of these materials which are key to these applications. A particular focus remains around the operating temperature, where there is a desire to produce materials with stable permittivity at high temperature ranges (e.g. 100–500 °C). A possible set of candidate materials are relaxor-like materials.

In conventional ferroelectric materials, when the temperature gets near to a phase change, a phonon softening allows the ready movement of the ions along the field direction leading to a substantial peak in the permittivity profile. Relaxors show a different behavior. This is characterized by particular features: a frequency dependence in the temperature maximum (T_{max}) of the permittivity peak; a slim polarization-Electric field (P-E) hysteresis loop; no clear structural transition at T_{max}; a deviation from the Curie–Weiss law; and the potential formation of polar domains above T_{max}. The exact origins of these effects and an entirely accepted scientific model remain debated in the literature e.g. [2–4].

From the wide range of relaxor-like materials available a particularly exciting set have been identified around $BaTiO_3$ (BT) perovskites with the addition of Bi-based perovskites including $BaTiO_3$-$Bi(Zn,Ti)O_3$ (BT-BZT) [5], $BaTiO_3$-$BiScO_3$ (BT-BS) [6], $BaTiO_3$-$Bi(Mg,Ti)O_3$ (BT-BMT) [7,8] and $Ca_{0.2}Ba_{0.8}TiO_3$-$Bi(Mg,Ti)O_3$ (BCT-BMT)[1]. These materials generate relatively flat permittivity-temperature profiles at high temperatures (e.g. above 100 °C) with the correct composition.

These materials are part of a wider trend in functional ceramics towards mixed-site compositional complex materials [9] for a range of applications such as high energy storage/discharge [10], thermoelectrics [11] and batteries [12]. These materials are highly dependent on multiple cations on sites and therefore have significant potential links to high entropy ceramics [13]. The formation of these materials relies on a complex interplay between mixing enthalpies and entropy [14–17]. Understanding of this is required to properly explore this materials space and generate the next generation of materials.

Although all different, the relaxor-based materials share similar themes in their processing, structure, and properties which are worth discussing collectively to understand the underlying chemistry and physics present. At large Bi-based contents (e.g. 33% in BT-BZT [5]) mixing results in multiple phases, but these values are far higher than the solubility of Bi in BT, demonstrating that the additional B site cations are facilitating the mixing [6]. Despite the appearance of single phases at low concentrations these are difficult materials to process [1] and there is evidence of incomplete reactions in what appear as single-phase samples for BCT-BMT [18] and BT-BZT [19]. Another interesting feature has been the observation of core-shell structures in BT-BS [6], indicating issues with the mixing of the materials. Still, these were only seen at lower levels of BS content. In BT-BZT such features were also noticed at higher content of BZT [19]. These features do not appear to link to separate electrical domains but do suggest potential issues with

* Corresponding author.
E-mail address: c.l.freeman@sheffield.ac.uk (C.L. Freeman).

https://doi.org/10.1016/j.actamat.2022.118649
Received 27 September 2022; Received in revised form 14 December 2022; Accepted 19 December 2022
Available online 20 December 2022

homogeneous mixing of the materials.

Structurally the materials show a tetragonal cell associated with BT at low Bi content which then shifts to a psueodcubic cell with increasing Bi content [1,5–8]. Detailed analysis of the structure of BT-BZT by Beuerlein et al. [19] using pair distribution function (PDF) analysis highlighted the structural variation that exists over the length scale of the view. At small length scales, even at higher Bi content, the material appears tetragonal but as the viewing length increases there is a shift to what appears pseudocubic. The suggestion is that these materials have local tetragonal regions which are disrupted by cubic regions or varied domain orientation of the regions. Analysis of the structures has shown the off-centered movement of Bi and Ti ions from their lattice sites [20] in BT-BS and Bi in BT-BZT [19] highlighting the distortion of the local lattice. Dynamic PDF has potentially refined this to suggest that the tetragonal cell may be a time averaged structure with a rhombohedral cell as the instant structure [21].

Electrically these materials show variation with the Bi content. At very low Bi content the materials appear ferroelectric with broad permittivity-temperature peaks. As the Bi content increases, classic relaxor-type behavior is observed with a frequency-dependent permittivity peak. This peak broadens with increasing Bi content and eventually a near flat permittivity is observed at temperatures above the peak. Several suggestions have been made to explain these features. The chemical heterogeneity could lead to the isolation of polar nano regions, which would alter the polarization process by fully decoupling them in BCT-BMT [18]. Alternatively, a potential correlation between ion relaxations in BT-BS has been suggested in the rattling ion type model [20]. The presence of the Bi moving off-center has been highlighted by Pramanick et al. which creates regions of intrinsic local modes which disrupt the basic softening modes of the ferroelectric (Ba,Ca)TiO_3 phase at higher content [21].

What is clear is that atomic-scale relaxations and arrangements play a key role in the large-scale dielectric properties of the materials, highlighting the need for atomic-scale resolution of these systems. Computer simulations have the advantage of providing that detailed resolution. What is also clear is the need to consider a wide range of atomic arrangements on the lattice to account for the structural diversity present in these materials, and to use large enough configurations to break artificial periodic effects and allow extended long-range structural relaxations. Here we use classical atomistic simulations methods to examine the BCT-BMT solid solution across a range of compositions from x= 0.01 to 0.55. Thousands of configurations are examined at each composition to provide an ensemble view of the system. We can draw energetic and structural detail about this system from this extensive sampling. We then use molecular dynamics simulations to study the polarization effects in these systems to identify how the local relaxations affect the polarization process(es) and the potential formation of polar nanoregions. We use this to explain the observed dielectric properties of these materials.

2. Theoretical section

All energy minimization calculations were performed using the GULP simulation package [22]. Forcefield parameters for Ba, Ti, Ca and O were taken from previous publications [23–25] which we have shown to be reliable for the structural and energetic properties of these perovskite systems. The parameters for Bi and Mg were fitted specifically for this publication and the values can be seen in Table S1. Note that all ions used a core model only with no shell to reduce the computational load of the simulations. Therefore, all core and shell charges were combined as one full valence ion and forcefield terms were all assumed to operate on the core of the ion.

For fitting the Bi-O interactions we followed a similar procedure to that outlined in our previous publication [23] where we fitted two crystal structures at the same time (α and δ-Bi_2O_3), fitting both the structure and the lattice energy, this ensured that our forcefield reported α-Bi_2O_3 as the most stable oxide form. For this purpose, we used the O-O interaction used in our other forcefield sets. Due to the size and number of simulations that would be performed for the BCT-BMT mix we deliberately fitted with no shell interaction to ensure the cost of the simulations would be viable later on. MgO forcefields are readily available in the literature (including within the Lewis and Catlow set [25]) which model MgO very well. When we tested these forcefields within our (and other $BaTiO_3$ forcefields) we found that these parameter sets showed a strong energetic preference for doping the Mg onto the A site. Although there is evidence in experimental studies that Mg can be doped onto the A site of $BaTiO_3$ [26] using careful compositional mixing, there is a preference for doping on the B site [27]. We verified this result with the use of DFT simulations using the CASTEP code [28] (ultrasoft pseudopotentials with 560 eV cutoff, gamma point, $4 \times 4 \times 4$ cell with 320 ions, full geometry optimization) which showed a clear energetic preference for B-site doping with Oxygen loss compensation versus the isovalent A site doping by 0.22 eV (per formula unit). Therefore, we refitted the Mg-O interaction focusing on producing the correct energetic preference for doping in $BaTiO_3$. It should be stressed that the parameters produced for MgO are only suitable for this specific case of B-site doping and not necessarily for general use in other ceramic systems.

Mixing of BMT into BCT was achieved using a monte carlo algorithm with the standard metropolis function. Each monte carlo run started from a random arrangement of the cations on their respective sites (i.e. Bi, Ba and Ca on the A site, Mg and Ti on the B site). The structure was then energy minimized. The following basic process was used which is visually represented in SI Fig. S2.

1 An A or B site cation is randomly selected, the position of this ion is swapped with a different type of atom from the same type of site (e.g. if a Ti was selected it was randomly swapped with a Mg).
2 Minimize energy of new configuration.
3 Compare optimized energy of new configuration with original configuration.
4 If the energy of the new configuration is lower than the original configuration then the swap is selected and the original configuration replaced with the new one. If the energy is higher then the difference between the energies is calculated and compared to a random number. If the difference is smaller than the random number then the swap is selected and the original configuration is replaced with the new one. If the difference is larger (or equal to) the random number then the swap is rejected and the original configuration is kept.
5 Return to step 1 using either the original configuration or the new one based on the outcome of step 4. In all cases store the data on the new configuration even if the swap is ultimately rejected.

Configurations were selected as viable when the configuration reached a stable minima and/or the gnorm for the optimization was 0.1 or below. Four separate monte carlo runs were attempted for each composition studied to generate a total of 2000 different configurations. Each cell contained $A_{216}B_{216}O_{648}$ ions.

Molecular dynamics simulations were performed using the DL POLY classic package [29]. Cells containing 1728 formula units (total 8640 ions) were generated from the two most energetically stable configurations. These were run using an NPT ensemble with 0.1 ps relaxation to hold the temperature and pressure at 300 K and 1 atm, respectively. The timestep was 0.5 fs. A range of electric fields were applied until polarization of the cell was observed with a field of 2.5 kVm^{-1}. Note this field is larger than those used in experimental systems. As the cell lacks any interfaces which could be the nucleation point for a polarization process and the classical simulations will not include all the higher order polarization terms associated with the alignment of the electron density we would expect the system to require a greater field to induce polarization. These simulations can therefore be viewed as a process to understand

the response to an electric field but the absolute numerics should not be expected to directly correlate to the real experimental systems. polarization vectors were calculated for each A and B site cation by comparing the actual position of the ion with the ideal central point of the surrounding polyhedra created by the neighboring Oxygen ions.

3. Results and discussion

3.1. Energetics and thermodynamics

The mixing energy calculated by considering the reaction scheme shown in Eq. (1) and using the most stable configuration obtained for each composition in our monte carlo search is shown in Fig. 1. This scheme minimized the energy of the left-hand side of the equation.

$$xBaTiO_3 + yCaTiO_3 + vMgO + zBi_2O_3 + (w-x-y)TiO_2 = Ba_xCa_yBi_zTi_wMg_vO_{648} \quad (1)$$

Mixing of all the compositions is unfavorable (positive) with a small increase in the energetic penalty as more BMT is mixed into the composition. This is the expected behavior of a mix where the enthalpy penalty increases as the two systems are combined. It is, however, interesting to note that the energy increase is small across the join and the penalty for a 0.55 mole fraction addition is not much larger than for a 0.01 mole fraction (0.52 vs 0.62 eV) where we might expect a more substantial energy penalty.

During the Monte Carlo search many of the configurations failed to optimize successfully, and therefore these arrangements of the ions are fundamentally unstable and do not represent viable configurations. This is due to the close proximity of particular cations, e.g. too many Bi around a Ti etc. The percentage of non-viable configurations identified during our sampling for each composition is shown in Fig. 2. When mixing a solid solution we expect to form an ideal or near-ideal solid solution where a large range of symmetrically unique configurations exist with similar energies. Below 0.15 mole fraction a large amount of variation in failed compositions with an average of ~15% is observed. This suggests these materials are difficult to mix. The natural ion migration and sintering process will be inhibited by the atomic arrangements that are energetically non-viable. With a further increase in the BMT content there is a rapid increase in the percentage of failed compositions up to ~70% at ~0.5–0.55 BMT. Therefore, beyond the small mixing composition this suggests a vast range of the potential configurations cannot form and therefore it will become difficult to achieve a single-phase material when mixing. We can further explore this effect by examining the availability of the configurations within the solid solution. As indicated, an ideal or near-ideal solid solution should have the majority of the states accessible within the mix. We can test this by calculating the energy difference between each configuration and the lowest energy configuration for that mix and compare this to the ambient heat available i.e. k_BT (where k_B is the Boltzmann constant and T is the temperature - assumed to be 1600 K based on the standard sintering conditions for these materials).

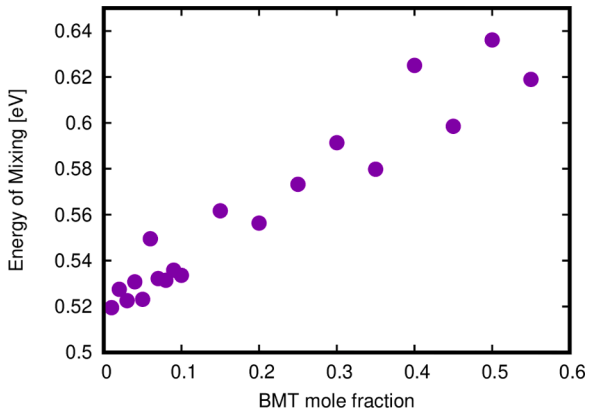

Fig. 1. Plot of energy of mixing for BCT-BMT with energies given per A site.

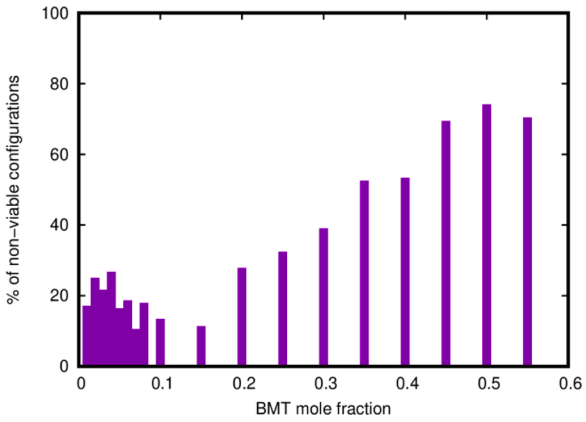

Fig. 2. Plot of percentage of non-viable configurations that failed to optimise during simulations.

We have combined the data for the number of configurations within 10 kBT of the lowest energy configuration with the data for non-viable configurations to calculate the percentage of configurations that might be occupied at each mix as shown in Fig. 3. We can immediately see how this percentage rapidly decreases with increasing BMT content and becomes a single digit beyond 0.05 BMT demonstrating that the BCT-BMT mix is far from ideal. There is speculation in highly disordered materials with multiple components that the entropy gain of mixing may offset the penalty from the enthalpy of mixing, so-called high entropy materials [9]. In the case of BCT-BMT the system does not gain a lot of entropy from the mixing process as many configurations are not viable or accessible and therefore this material cannot be considered to be a high entropy ceramic where entropy is key to stabilizing an enthalpic mixing penalty [14,17].

Taken together, the energetic information provides an interesting pattern of information about the BCT- BMT solid solution.

- At low BMT content (up to ~0.1 BMT) a more traditional defect/solid solution type of mixing occurs. There is a large enthalpic penalty associated with mixing BMT into the BCT system but this generates multiple possible configurations. We can consider x=0.1 as a conventional solid solution limit. Mixing will therefore be difficult which relates to experimental findings e.g. [1] but can be achieved and should generate a relatively wide range of potential structures

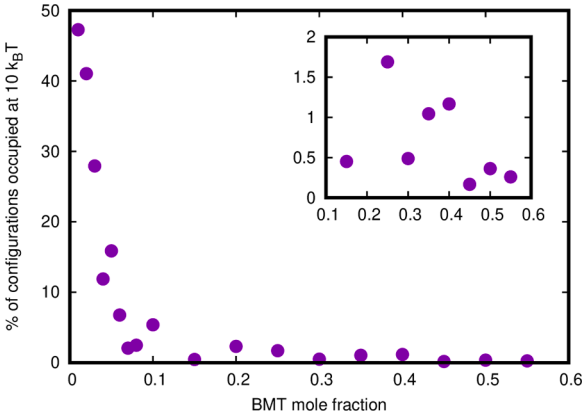

Fig. 3. Plot of % of potentially occupied configurations (with 10 k_BT ambient energy) with BMT mole fraction. Inset shows 0.10 to 0.55 mole fraction of BMT on a reduced scale.

with a range of different local geometries and behave more like a traditional solid solution. We might expect to observe the formation of micro-segregation in these region as incomplete diffusion takes but a general continuous mix is achievable.

- With higher BMT contents we find increasingly more configurations that will not mix at all but that very specific arrangements of the ions which have smaller enthalpic penalties can occur. Therefore, in this region we will see a nanoscale segregation that would be associated with these more specific atomic arrangements and not a general heterogeneous features (those configurations will simply fail to mix). This suggests making these materials will be extremely challenging as is seen in experimental processing.

3.2. Structure

The difference between structural order at various length scales has been analyzed experimentally using PDF in other relaxor-like materials [19,21]. These have indicated that a short-range view of the material shows tetragonal or rhombohedral unit cells in these materials but at longer ranges these cells will average out to be pseudocubic. We have performed a similar analysis on our simulation cells as presented in Fig. 4. Here the simulation cells are divided into smaller cells of a single unit cell length (i.e. one A-A site separation), three and six unit cells. We then examine the lattice parameters and angles for each of these cells and define the reduced cells as orthorhombic, tetragonal or cubic. The total number of each type of cell can then be counted and reported as a fraction of all the total number of reduced cells. These results show how as the view length increases (i.e. the larger the divided cell) from top to bottom in Fig. 4 there is an increasing percentage of cells defined as cubic within the system. This follows a similar pattern to that observed in experiments. So at a local level, a cell may appear non-cubic but the cell would appear cubic with a larger view. Across the mixing range, the added BMT stabilizes the orthorhombic and tetragonal cells as the Bi and Mg ions drive distortions. This suggests the size of the distorted regions are growing within the cell as the BMT content increases.

To further explore the structures we collected various coordination data. [18] reported a segregation of Ba-Ti rich regions and Bi-rich regions in the x=0.55 composition. Due to the necessity of charge balancing they suggested that the Bi-rich regions would also be Mg-rich. Within the composition we would expect Mg^{2+} cations to cluster around Bi^{3+} cations to reduce the Coulombic repulsion associated with neighboring Bi^{3+}-Ti^{4+}. We observed a small tendency for Bi to neighbor to Mg. We do not see a clear tendency for Ba-Ti segregation (see SI Fig. 1). We suggest that the potential segregation observed in experimental samples would link to the previously reported non-viable configurations. In these regions, poorly formed material that is not fully mixed is obtained. This would not be detected as a separate phase as it will represent small deviations from the desired mix and could be more viewed as nano segregation discussed in some perovskite mixes.

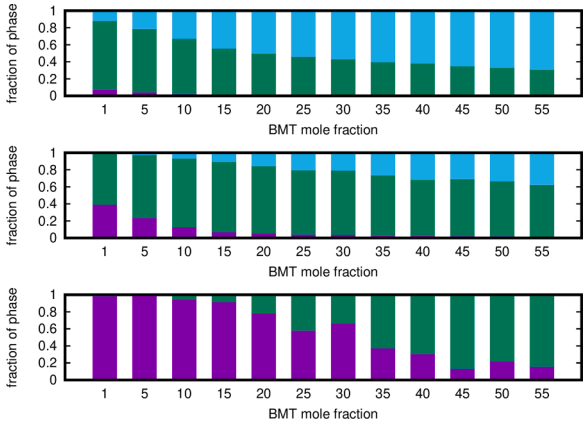

Fig. 4. Fraction BCT-BMT cells showing cubic (purple), tetragonal (green) and orthorhombic (blue) cells at a single unit cell length (top), three unit cells length (middle), and six unit cells length (bottom) across the composition range (For interpretation of the references to color in this figure legend, the reader is referred to the web version of this article).

Examination of the local coordination of the cations with Oxygen (see Table 1) shows that the mean A-site cation to O separations increase with the BMT content whereas the B-site cation to O separations decrease. The standard deviations of these separations indicate that the coordination shells become increasingly varied, particularly on the A-site, as the BMT content increases. The BaO and CaO distributions widen significantly (with the deviation becoming 0.25 and 0.39 Å, respectively) and a range of different Ca-O and Ba-O separations are present. Closer inspection of individual cation sites shows these correspond to a range of different cation-O environments i.e. each A-site can have slightly different combinations of Ca-O or Ba-O separations.

The Bi-O separation behaves differently, Fig. 5. At low BMT content (0.01-0.1) this shows one dominant peak at 2.7 Å and small peaks at 2.5 and 2.95 Å. Examination reveals this stems from two different BiO environments. One with all the Bi-O separations similar and around 2.7 Å and another with a 3x short, 6x medium and 3x long Bi-O separations. These later cases occur when a Mg is nearest neighbor to the Bi. This suggests that the presence of the Mg facilitates the Bi to move off center within its A-site. As we increase the BMT content the frequency of the shorter peak for BiO at 2.5 Å increases whereas the longer peak decreases. Examination of individual configurations reveals we are now beginning to see a variety of different Bi-O environments forming with a preference for shorter Bi-O separations as more and more Bi ions move off the centre of their site. Once again this appears to be linked to the presence of Bi-Mg neighboring sites. Beyond x=0.1 the peaks overlap and the mean Bi-O separation increases due to the maximum Bi-O separation increasing. Beyond x=0.3 the broad Bi-O peak refines and one major dominant peak occurs at about 2.5 Å and a further peak at about 3.2 Å. This structure relates to an 8x short and 4x long Bi-O coordination. As we increase the BMT content further the Bi all become neighbors to Mg cations. This can therefore be viewed as a percolation process where we need a large enough number of Bi and Mg present to find each other and to enable the relaxations around the Bi site.

The B-site cations, Mg and Ti, have a much narrower B-O

Table 1
Average inter-atomic separations (with standard deviation) at different mole fractions of BMT.

BMT mole fraction	Average Cation-O 1st coordination shell separation Å				
	Ba-O	Ca-O	Bi-O	Mg-O	Ti-O
0.01	2.83 ± 0.04	2.79 ± 0.08	2.69 ± 0.05	2.10 ± 0.02	1.99 ± 0.01
0.05	2.83 ± 0.07	2.80 ± 0.16	2.69 ± 0.11	2.09 ± 0.03	1.99 ± 0.01
0.10	2.84 ± 0.10	2.81 ± 0.21	2.69 ± 0.15	2.09 ± 0.05	1.99 ± 0.02
0.15	2.84 ± 0.12	2.82 ± 0.25	2.70 ± 0.19	2.09 ± 0.05	1.98 ± 0.02
0.20	2.85 ± 0.15	2.83 ± 0.29	2.71 ± 0.23	2.09 ± 0.06	1.98 ± 0.02
0.25	2.86 ± 0.17	2.83 ± 0.31	2.72 ± 0.20	2.08 ± 0.06	1.98 ± 0.02
0.30	2.86 ± 0.18	2.84 ± 0.32	2.72 ± 0.28	2.08 ± 0.07	1.98 ± 0.02
0.35	2.87 ± 0.20	2.85 ± 0.34	2.73 ± 0.30	2.07 ± 0.07	1.98 ± 0.03
0.40	2.87 ± 0.21	2.85 ± 0.37	2.73 ± 0.31	2.07 ± 0.08	1.97 ± 0.03
0.45	2.87 ± 0.22	2.85 ± 0.37	2.73 ± 0.33	2.07 ± 0.08	1.97 ± 0.03
0.50	2.88 ± 0.23	2.85 ± 0.38	2.74 ± 0.34	2.06 ± 0.08	1.97 ± 0.03
0.55	2.88 ± 0.25	2.86 ± 0.39	2.75 ± 0.36	2.06 ± 0.09	1.97 ± 0.03

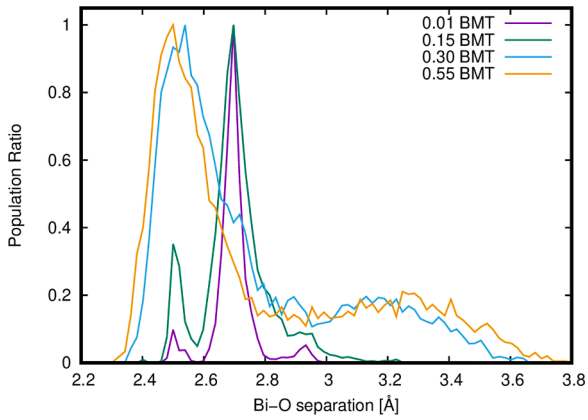

Fig. 5. Plot of the distribution of Bi-O separations at different BMT mole fractions. The frequencies of the different separations are all scaled with the most frequent separation with a value of 1.

distribution. For Ti-O the separation shrinks and broadens slightly as the BMT content increases. For MgO there is also a gradual shrinking but inspection of the distribution shows this relates to a change in the coordination shells from regular octahedra (Fig. 6). As the BMT content increases, a single Mg-O separation increases and some shrinkage of the remaining 5 Mg-O separations occurs around the cation. This process is gradual but becomes more dominant at 0.45 BMT mole fraction when the peak for the shorter separations moves significantly from ~2.1 to ~2.0 Å

Following the structural changes with BMT content it is clear to see that the A-site is much more deformed with increasing BMT content. The larger A-site allows for more distortion of the cation-Oxygen separation. The movement of the Bi off-center will push neighboring Ca and Ba off-center. The other A-site relaxations, however, are not regular and produce a range of different environments. Each Ca or Ba is relaxing in response to their local environment, e.g. Bi, Mg, Ti, etc. This induces other relaxations in the other surrounding A-site cations. This helps explain why a clear energy correlation is not observed for Bi to Mg coordination as might be expected in more conventional defect chemistry. Although Bi-Ti neighbors are generally unfavorable this pairing can be mitigated by, for example, Ca ions that can shift off-center to reduce Coulombic repulsion. Therefore, what we are observing in this system is a set of interlinked local structures, i.e. the energetics of a site depends not only on the first neighbors but also the second and third neighbors, i.e. specific arrangements and relaxations of the ions that help stabilize specific local structures. So we expect to have particular local structure motifs that might be regularly observed but no clear simple repeat periodicity. This again connects to the symmetry of the unit cells compared to the viewing length in Fig. 4 where we observed increasing the BMT content increased the deviation within the structure. Structurally we can identify three different regions in our BCT-BMT mixed material.

- At low BMT content (up to 0.1) we see a more regular solid solution type of behavior. The structure is effectively that of BCT. Small local disruptions are occurring in the lattice caused by the BMT content but the majority of the ions remain in the center of their sites. This correlates to the same region identified energetically.
- As the BMT content increases (from 0.1 to 0.45) we see increasing structural distortions centred around the Bi and Mg imposing their preferred coordination onto the structure. This generally involves pushing cations off-center within their sites. The Bi ion achieves this firstly around 0.3 BMT, then the Mg around 0.45 BMT.
- At large BMT content (0.45–0.55) the Bi and Mg reach a percolation limit where they are now coordinated regularly with each other and have imposed relaxations across all the cation sites. This has led to a very particular arrangement of all the ions in the material.

3.3. Dielectric properties

With an in-depth analysis of the structure completed it is appropriate to examine the effect of these structures on the polarization of the material. As discussed in the methods section we have performed a range of molecular dynamics simulations on different BCT-BMT mixes with and without an electric field applied to the system.

Therefore, we have extracted the localized polarization vectors around each A and B lattice site. We analyzed the alignment of these polarization vectors between neighboring A and B-sites, with and without the applied electric field, by calculating the dot product of neighboring vectors on each of the A and B-sites. An angle of 0° indicates perfect alignment between the neighboring dipoles, an angle of 90° indicates they are orthogonal to each other and an angle of 180° indicates they are anti-parallel. The frequency of observing each angle was then recorded throughout the simulations. Note that in the presence of no field the cell has no overall dipole but small localized dipoles will continually form throughout the simulation due to the natural movement of the ions.

The average response for a range of configurations with varying amounts of BMT is shown in Fig. 7. For all levels of BMT there is little alignment of the neighboring polarization vectors. The distribution is that of a random set of vectors with a maximum at ~ 90°. The polarization vectors created by the cations are therefore unaffected by those of

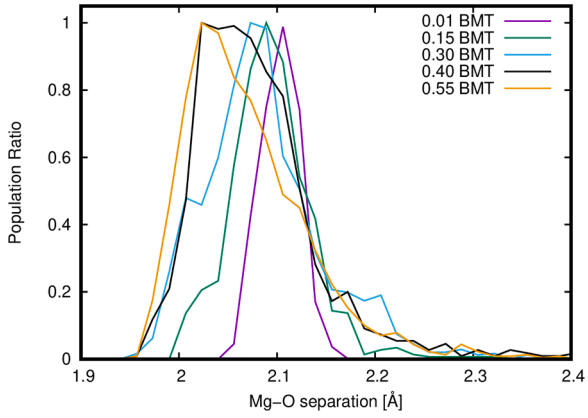

Fig. 6. Plot of the distribution of Mg-O separations at different BMT mole fractions. The frequencies of the different separations are all scaled with the most frequent separation with a value of 1.

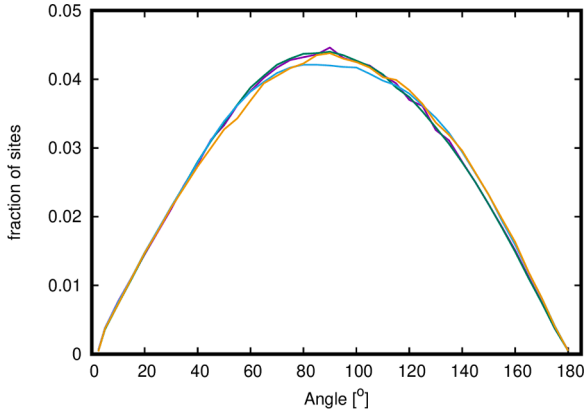

Fig. 7. Plot of alignment of neighboring ionic dipoles with no electric field. BMT mole fraction 0.05 (purple), 0.15 (green), 0.30 (blue), 0.50 (orange) (For interpretation of the references to color in this figure legend, the reader is referred to the web version of this article).

their neighbors and there is no formation of localized domains or order.

Different behavior occurs when the system is subjected to an electric field, Fig. 8. For 0.05 BMT content the ions are largely aligned parallel or anti-parallel to the field but this is gradually lost with increasing BMT content. We visualize this process in Fig. 9 which color codes the polarization direction of B-sites. Where the colors are similar, we observe alignment with the field that is clear at 0.1 BMT with small units breaking up these regions. As the BMT content increases we see a more random pattern of colors implying sites are not generally aligning.

The alignment of Ti polarization vectors with electric field is shown in Fig. 10. These are largely anti-parallel (i.e. 180°) at low BMT content (which reflects the positive Ti moving toward the negative pole) but this angle reduces with increasing BMT content and at 0.5 BMT there is a substantial number that are orthogonal to the field. The response of the Bi (Fig. 10) is more telling. There is parallel alignment at low BMT but a smaller quantity that does not align (the region around 90°). As the Bi is too small for the A-site it should be able to rattle and move under a field, however, as we highlighted in our structural examination there are two-environments for the Bi cation. When it sits more centrally within the A-site, it can move with the field and polarize, but when it naturally relaxes to an off-centered position, moving the cation due to the field will be harder due to its strong ionic relaxations. A small quantity of the off-centered Bi (generally coupled to Mg) appears to disrupt the field's alignment. As the BMT content increases and the number of off-centered Bi sites increases, the alignment decreases until it is nearly a random distribution at x=0.5. Similar behavior can be observed for the Mg polarization vectors although the loss of alignment with the field is more gradual than for the Bi cation as highlighted in the structural analysis.

We also examined how temperature may alter the response of the ions to the field by performing additional molecular dynamics simulations at 400 and 500 K. Phase changes in materials are extremely challenging to model and the changes that occur are clearly very small in the BCT-BMT system. As a consequence, we did not observe any significant structural changes in our simulations beyond a small thermal expansion of the lattice. As temperature increases we would, however, expect a breakdown in alignment of the ions with the field. Greater thermal energy should lead to more random relaxations of the ions as the system becomes paraelectric.

The fraction of Ti cations aligned anti-parallel (at an angle of 150–180°) with the field at different temperatures is shown in Fig. 11. For 0.05 BMT the expected behavior is observed; as temperature increases alignment is lost indicating the material will not respond as well to the field. For 0.50 BMT the lower levels of alignment do not change with temperature. This behavior stems from the distinct relaxations that have taken place in the material that prevent significant movement of the ions. Therefore there is little movement of the ions to be disrupted and randomized with thermal energy (as in the case at low BMT content) nor does the extra thermal energy help move the ions out of their relaxed positions to enable them to align with a field. This suggests the polarization (and therefore measured permittivity) of the material will fluctuate less with the temperature as is observed experimentally.

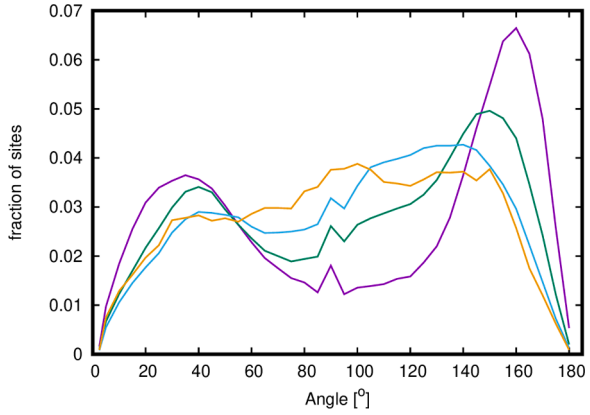

Fig. 8. Plot of alignment of ionic dipoles with electric field. BMT mole fraction 0.05 (purple), 0.15 (green), 0.30 (blue), 0.50 (orange) (For interpretation of the references to color in this figure legend, the reader is referred to the web version of this article).

Treating our analysis together and comparing it to the experimentally recorded dielectric properties that have been reported we can construct a model for the BCT-BMT system which we represent in Fig. 12.

- At low BMT content we see a system relating to a more conventional solid solution where ions remain largely centered in their sites and the structure is mostly following a BCT lattice. When this system is subjected to an electric field the ions will polarize with the field. This follows a conventional phonon-softening process observed in conventional ferroelectrics with a peak occurring around the phase transition. The peak is broadened by the chemical and structural heterogeneity of the system but the temperature of the peak maximum does not shift with frequency as the polarizing regions are all interconnected and we do not have isolated (polar nano) regions.
- As the BMT content increases we now see the breakdown of the solid solution and the formation of larger relaxations in the structure as the Bi and Mg force the relaxations of the system. For x = 0.1-0.4 BMT content, these relaxations create localized regions. The relaxations within these regions are strong which means the cations will not readily align with an electric field. This will decrease the overall permittivity of the material as the BMT content increases. The presence of these regions and sites will isolate sections of the structure which still maintain the more conventional BCT structure. These become the polar nanoregions associated with relaxor-type behavior. They will polarize with the electric field but due to the variation in their size and chemistry the polarization and relaxation occurs across a range of frequencies.
- When the BMT content reaches x=0.45 and above the percolation of Bi-Mg is fully achieved and all the ions are pushed into localized relaxations. This essentially shrinks the polar nanoregions to atomic sizes and therefore no large scale polarization alignment is possible within the material and the permittivity shows essentially no peak as the ions do not respond easily to an electric field. The permittivity therefore essentially appears largely flat across the temperature range as connected polarization is suppressed within the material.

We can see clear parallels between our findings with other suggested models for these relaxor-like materials. Pramanick et al. [21] highlighted that the presence of Bi and Sc in Sn-doped BCT-BS disrupted the ability of the Ti to undergo softening modes. Roncal-Herrero et al. [18] highlighted the role of the Bi- Mg rich regions in isolating the polar regions. Our results expand these models by providing an atomic view of the system. We can see that natural mixing coupled with local relaxations will create the necessary distribution of non-polarizing regions that will disrupt the formation of polar nanoregions. Our understanding of the BCT-BMT system is also applicable to other Bi-based high T relaxor ferroelectrics. The difference in the exact response will vary. For example 1) 3+ valence cations (e.g. Sc) are used on the B site and therefore relaxations on a whole may be smaller 2) the lack of the smaller Ca^{2+} cation on the A-site that facilitates relaxations and mixing in the BCT-BMT system may mean that greater concentrations of Bi-based material cannot be reached 3) different nano and micro-segregation could take place due to the ability of the phases to mix and the different atomic scale relaxations. These results also suggest that a general disruption of the A site behavior through doping or other defects in a range of perovskites could facilitate a smaller scale version of these effects by causing B site cations to substantially relax inhibiting their response to an electric field.

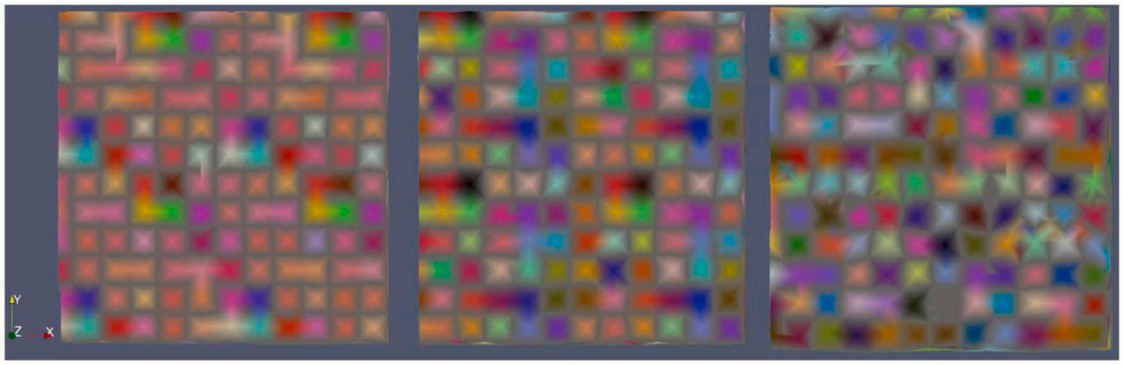

Fig. 9. polarization of B sites in a slice through BCT-BMT mix represented by color coding. Similar colors indicate alignment of polarization vectors. Left 0.1 BMT. Middle 0.3 BMT. Right 0.5 BMT.

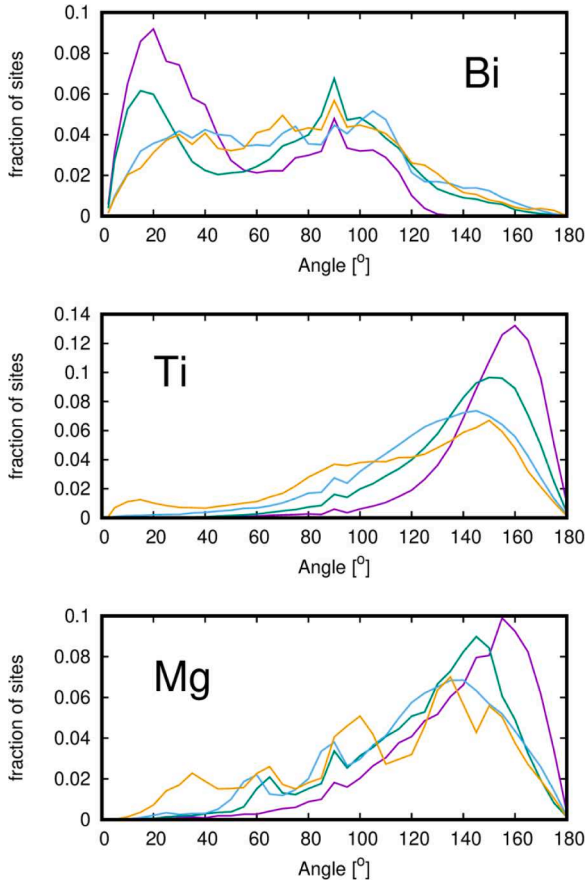

Fig. 10. Plot of alignment of dipoles of particular ion species with electric field. BMT mole fraction 0.05 (purple), 0.15 (green), 0.30 (blue), 0.50 (orange) (For interpretation of the references to color in this figure legend, the reader is referred to the web version of this article).

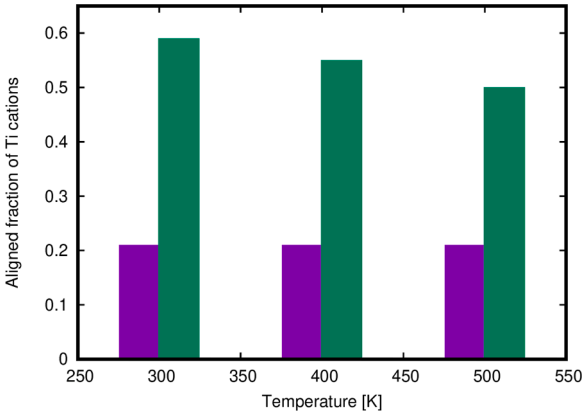

Fig. 11. Fraction of Ti cations aligned anti-parallel with the field (within 30°) for BMT mole fraction 0.05 (green) and 0.50 (purple) at temperatures 300, 400 and 500 K (For interpretation of the references to color in this figure legend, the reader is referred to the web version of this article).

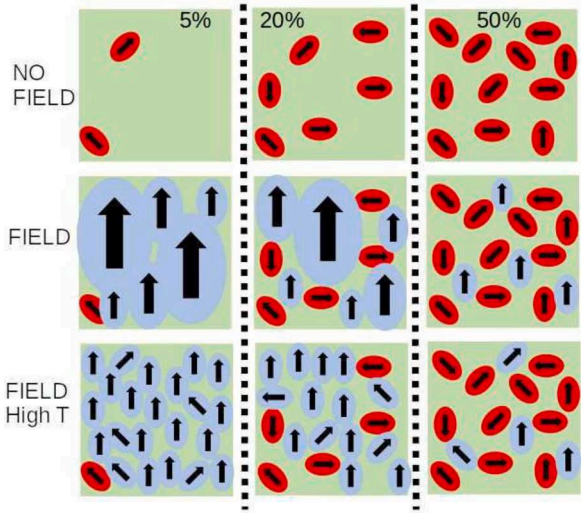

Fig. 12. Schematic representation of relaxation and polarization processes in the BMT-BCT system. Red regions represent localized relaxations from Bi and Mg. Blue regions represent polarization from an electric field. Rows show different conditions: Top no field applied; Middle field applied at lower temperatures (below T_{max}); Bottom field applied at higher temperatures (above T_{max}). Columns depict different amounts of BMT: Left 0.05 BMT; Middle 0.2 BMT; Right 0.5 BMT (For interpretation of the references to color in this figure legend, the reader is referred to the web version of this article).

4. Conclusions

We have performed a set of classical simulations to study the BCT-BMT solid solution and used these simulations to understand the energetics, structure and dielectric behavior of this material. Our study demonstrates (1) that the BCT-BMT system changes from a more conventional solid solution at very low BMT content into a highly non-ideal mix where only particular atomic arrangements are observed. (2) As the BMT content increases there is a gradual shift towards percolation of Bi and Mg in the lattice which causes strong local relaxations of the ions into small polarized units. (3) The localized relaxations of these ions

disrupts the ability of the material to polarize with an electric field. (4) This disruption of the polarization leads to the relatively flat temperature-permittivity profiles observed experimentally in these relaxor-like ferroelectric materials.

Supporting information

Supporting Information is available from the Elsevier Online Library or from the author.

Declaration of Competing Interest

The authors declare that they have no known competing financial interests or personal relationships that could have appeared to influence the work reported in this paper.

Acknowledgments

This research was supported by the "Analysis of Polar Nanostructures in High Temperature Relaxor Dielectrics: a Framework for Materials Discovery" grant (EPSRC grant EP/P015565/1) and the "Substitution and Sustainability in Functional Materials and Devices" grant (EPSRC grant EP/L017563/1). *Via* our membership of the UK's HEC Materials Chemistry Consortium, which is funded by EPSRC (EP/R029431), this work used the ARCHER UK National Supercomputing Service (http://www.archer.ac.uk). For the purpose of open access, the author has applied a Creative Commons Attribution (CC BY) licence to any Author Accepted Manuscript version arising from this submission

Supplementary materials

Supplementary material associated with this article can be found, in the online version, at doi:10.1016/j.actamat.2022.118649.

References

[1] A. Zeb, S.J. Milne, Stability of high-temperature dielectric properties for (1-x) $Ba_{0.8}Ca_{0.2}TiO_3$-xBi$(Mg_{0.5}Ti_{0.5})O_3$ ceramics, J. Am. Ceram. Soc. 96 (9) (2013) 2887.
[2] B. Hehlen, M. Al-Sabbagh, A. Al-Zein, J. Hlinka, Relaxor ferroelectrics: back to the single-soft-mode picture, Phys. Rev. Lett. 117 (2016) 15.
[3] H. Takenaka, I. Grinberg, S. Liu, A.M. Rappe, Slush-like polar structures in single-crystal relaxors, Nature 546 (2017) 391–395.
[4] A. Glazounov, A. Bell, A. Tagantsev, A. Tagantsev, Relaxors as superparaelectrics with distributions of the local transition temperature, J. Phys. Condens. Matter 7 (21) (1995) 4145.
[5] C.C. Huang, D.P. Cann, Phase transitions and dielectric properties in Bi$(Zn_{1/2}Ti_{1/2})O_3$ – $BaTiO_3$ perovskite solid solutions, J. Appl. Phys. 104 (2008) 2.
[6] H. Ogihara, C.A. Randall, S. Trolier-McKinstry, Weakly coupled relaxor behavior of $BaTiO_3$ –$BiScO_3$ ceramics, J. Am. Ceram. Soc. 92 (1) (2009) 110.
[7] B. Xiong, H. Hao, S. Zhang, H. Liu, M. Cao, Structure, dielectric properties and temperature stability of $BaTiO_3$ –Bi$(Mg_{1/2}Ti_{1/2})O_3$ perovskite solid solutions, J. Am. Ceram. Soc. 94 (10) (2011) 3412.
[8] Q. Zhang, Z. Li, F. Li, Z. Xu, Structural and dielectric properties of Bi$(Mg_{1/2}Ti_{1/2})O_3$–$BaTiO_3$ lead-free ceramics, J. Am. Ceram. Soc. 94 (12) (2011) 4335.
[9] A.J. White, J. Luo, A step forward from high-entropy ceramics to compositionally complex ceramics: a new perspective, J. Mater. Sci. 55 (2020) 9812.
[10] H. Pan, F. Li, Y. Liu, Q. Zhang, M. Wang, S. Lau, Y. Zhang, J. Ma, L. Gu, Y. Shen, P. Yu, S. Zhang, L.Q. Chen, Y.H. Lin, C.W. Nan, Ultrahigh–energy density lead-free dielectric films *via* polymorphic nanodomain design, Science 365 (2019) 578.
[11] P. Zhang, Z. Lou, M. Qin, J. Xu, J. Zhu, Z. Shi, Q. Chen, M.J. Reece, H. Yan, F. Gao, High-entropy $(Ca_{0.2}Sr_{0.2}Ba_{0.2}La_{0.2}Pb_{0.2})TiO_3$ perovskite ceramics with A-site short-range disorder for thermoelectric applications, J. Mater. Sci. Technol. 97 (2022) 182.
[12] Z. Lun, B. Ouyang, D.H. Kwon, Y. Ha, E.E. Foley, T.-Y. Huang, Z. Cai, H. Kim, M. Balasubramanian, Y. Sun, R.J. Clement, H. Ji, G. Ceder, Cation-disordered rocksalt-type high-entropy cathodes for Li-ion batteries, Nat. Mater. 20 (2021) 214.
[13] C.M. Rost, E. Sachet, T. Borman, A. Moballegh, E.C. Dickey, D. Hou, J.L. Jones, S. Curtarolo, J.P. Maria, Entropy-stabilized oxides, Nat. Commun. 6 (2015), 8485, https://doi.org/10.1038/ncomms9485.
[14] S.J. McCormack, A. Navrotsky, Thermodynamics of high entropy oxides, Acta Mater. 202 (2021) 1.
[15] S. Jiang, T. Hu, J. Gild, N. Zhou, J. Nie, M. Qin, T. Harrington, K. Vecchio, J. Luo, A new class of high-entropy perovskite oxides, Scr. Mater. 142 (2018) 116.
[16] K.C. Pitike, S. KC, M. Eisenbach, C.A. Bridges, V.R. Cooper, Predicting the phase stability of multicomponent high-entropy compounds, Chem. Mater. 32 (2020) 7507.
[17] G. Anand, A.P. Wynn, C.M. Handley, C.L. Freeman, Phase stability and distortion in high-entropy oxides, Acta Mater. 146 (2018) 119.
[18] T. Roncal-Herrero, J. Harrington, A. Zeb, S.J. Milne, A.P. Brown, Nanoscale compositional segregation and suppression of polar coupling in a relaxor ferroelectric, Acta Mater. 158 (2018) 422.
[19] M.A. Beuerlein, N. Kumar, T.M. Usher, H.James Brown-Shaklee, N. Raengthon, I. M. Reaney, D.P. Cann, J.L. Jones, G.L. Brennecka, Current understanding of structure–processing–property relationships in $BaTiO_3$–Bi$(M)O_3$ dielectrics, J. Am. Ceram. Soc. 99 (9) (2016) 2849.
[20] V. Krayzman, I. Levin, J.C. Woicik, F. Bridges, Correlated rattling-ion origins of dielectric properties in reentrant dipole glasses $BaTiO_3$-$BiScO_3$, Appl. Phys. Lett. 107 (2015) 19.
[21] A. Pramanick, S. Nayak, T. Egami, W. Dmowski, A.S. Budisuharto, F. Marlton, M. R. Jorgensen, S.Venkateshwarlu V, K.A. Beyer, Dynamical origins of weakly coupled relaxor behavior in Sn-doped (Ba, Ca)TiO_3 -$BiScO_3$, Phys. Rev. B 103 (2021) 21.
[22] J. Gale, A. Rohl, The general utility lattice program, Mol. Simul. 29 (5) (2003) 291.
[23] C.L. Freeman, J.A. Dawson, H.R. Chen, J.H. Harding, L.B. Ben, D.C. Sinclair, A new potential model for barium titanate and its implications for rare-earth doping, J. Mater. Chem. 21 (13) (2011) 4861.
[24] J.A. Dawson, X. Li, C.L. Freeman, J.H. Harding, D.C. Sinclair, The application of a new potential model to the rare-earth doping of $SrTiO_3$ and $CaTiO_3$, J. Mater. Chem. C 1 (8) (2013) 1574.
[25] G. Lewis, C.R.A Catlow, Potential models for ionic oxides, J. Phys. C – Solid State Phys. 18 (6) (1985) 1149.
[26] O. El ghadraoui, M. Zouhairi, F. Abdi, T. Lamcharfi, H. Bali, E.El ghadraoui, Preparation and physico-chemical physico study of Mg doped $BaTiO_3$ ($Ba_{1-x}Mg_xTiO_3$) prepared by the sol–gel sol method, Int. J. Curr. Res. 8 (12) (2016) 42815.
[27] H. Miao, M. Dong, G. Tan, Y. Pu, Doping effects of Dy and Mg on BaTiO3 ceramics prepared by hydrothermal method, J. Electroceram. 16 (4) (2006) 297, 3rd International Conference on Materials for Advanced Technologies (ICMAT-2005)/ 9th International Conference on Advanced Materials (ICAM 2005), Singapore, SINGAPORE, JUL 03-08, 2005.
[28] S. Clark, M.D. Seagall, C.J. Pickard, P.J. Hasnip, M.J. Probert, K. Refson, M. C. Payne, First principles methods using CASTEP, Zeitschrift fuer Kristallographie 220 (5-6) (2005) 567.
[29] W. Smith, T. Forester, A general-purpose parallel molecular dynamics simulation package, J. Mol. Graph. 14 (1996) 136.